Article | Received 31 October 2024; Accepted 2 March 2025; Published date
https://doi.org/10.55092/rl20250002

Design and fabrication of two-step expansion flexible gripper for dynamic grasping range †

Jingxiang Wang[1], Yangzesheng Lu[1], Chengqi Song[1], Bingjie Xu[2], Qinglei Bu[1,*], Jie Sun[1,*] and Quan Zhang[1]

[1]Department of Mechatronics and Robotics, Xi'an Jiaotong-Liverpool University, Suzhou, China
[2]School of AI, Suzhou Industrial Park Institute of Vocational Technology, Suzhou, China

† This manuscript is an extended version of the paper presented at the 2024 29th International Conference on Automation and Computing (ICAC) and has been granted copyright permission for publication.

* Correspondence authors; E-mails: Qinglei.Bu02@xjtlu.edu.cn (Q.B.); Jie.Sun@xjtlu.edu.cn (J.S.).

Abstract: With advancements in robotics, flexible robotic arms have increasingly become part of daily life, assisting or even replacing humans in various tasks across diverse environments due to their inherent safety and flexibility. To enhance the grasping capability of robotic arms and achieve a dynamic and wider grasping range, this study introduces the design, simulation, and testing of a two-step expansion flexible gripper featuring inflatable fingers and a pneumatic palm. The gripper's operation is supported by a pneumatic drive control system that is implemented using a solenoid valve. Compared to existing designs, the proposed gripper and corresponding two-step expansion control enable the gripper to effectively grasp objects with varying geometries and material hardness, offering improved adaptability and functionality. This paper is an extended version of [1].

Keywords: flexible mechanical gripper; pneumatic actuation; flexible inflatable palm; 3D printing

1. Introduction

The rapid development of autonomous guided vehicles has drawn a lot of interest [2,3], and they can be equipped with robotic arms and grippers to enhance their manipulating capabilities. Diverse robot arms and grippers have been developed for assembly, welding, material handling, and even surgery, which serve as programmable extensions of the human arm and fingers. The traditional robotic arms and fingers are made up of various rigid materials, e.g., metals and polymers. With a proper design, such robot arms and fingers can be used for consistent operation in a specific task. They also exhibit minimal deformation when subjected to external forces. Moreover, additional protection rules are applied so that they cannot reach and endanger operators. These factors may limit their applications, especially when faced with multi-tasks, resulting in a challenge in complex application scenarios.

Recently, the development of soft materials has attracted significant attention, particularly in the context of flexible robotic arms and grippers [4]. In general, they have better safety compliance when working in close contact with humans, and demonstrate the potential to outperform traditional rigid robot

Copyright©2025 by the authors. Published by ELSP. This work is licensed under a Creative Commons Attribution 4.0 International License, which permits unrestricted use, distribution, and reproduction in any medium provided the original work is properly cited.

arms and grippers in severing people for daily life [5–7].

The soft grippers may securely and reliably grasp a larger range of geometries than traditional rigid grippers. With simple control strategies, they can offer many grab modes and achieve the high degrees of freedom, which makes them perfect for goods handling. Various flexible robotic grippers have been designed and investigated due to their advantages, including overall lightweight, higher motion flexibility, and rapid response. A new pneumatic flexible actuator was developed by a research team that combined elongation, contraction, and bending functions [8]. This team tested a grasping and removal scheme as actuators for object movement. Another research team [9] has designed a gripper that can assist robots in reaching destinations safely in response to the problem of quadruped robots that cannot walk properly in harsh environments. In order to grasp fragile items underwater, an improved flexible robotic arm that integrates the mechanical sensors at the end of the arm has been designed [10], through the haptic feedback. When the inflatable fingers touch the object, they can achieve action planning in time to minimize the risk of breaking, which extends the application range in terms of underwater archaeology. In the agriculture scenario, a flexible gripper for harvesting and transporting thin-skinned fruits and vegetables is proposed [11], which can control the interaction force within a specific range under high acceleration without destroying the fruits or vegetables. In addition to the capability of being an assistant in daily life, the finger of flexible robotic arms occasionally appears in aerospace scenarios. One research team designed an ultra-high-degree-of-freedom flexible robotic arm bionic to the trunk of an elephant with eight flexible joints [12] to avoid obstacles. The flexible movement with a vast operating range provides a solid guarantee that the mission is completed. A research team improves flexible finger perception and control [13]. But it still requires manual adjustment of the adapter to change finger spacing for different tasks. This necessity for physical adjustment can limit its applicability in dynamic environments where the time and labor costs associated with changing adapters could be prohibitive.

Although soft grippers have made progress, their gripping capacity is still limited by the volume of their grasping workspaces and their ability to alter them for different activities. Most of the current grippers can merely grasp a single type of object, leaving the replacement of the gripper manually or adjustment of the mechanical buckle complicated. To overcome this issue, this paper proposes a novel soft gripper with a flexible palm, which can be controlled independently to not only capture different shapes of objects but also in an adjustable dynamic grasping range based on the scale. With the improvement of this structure, a two-step expansion algorithm is proposed to precisely adjust the grasping range based on different shapes of objects. The comparison between the simulation and experimental results of the variation has been tested to prove the effectiveness of the design.

2. Robotic arm with flexible gripper

Figure 1 illustrates the overall design, which includes two main sections: a robotic arm and a flexible gripper. The former involves structural design and control, which is related to the stepper motor and trajectory planning. In the structural design of the robotic arm, the motor is selected after calculating the maximum load and verifying its strength to ensure proper functionality. The main body of the robotic arm is produced using 3D printing technology, which helps reduce both costs and manufacturing time. The arm is controlled by stepper motors and simulated in MOVEIT2 environment. In terms of the gripper, which focuses on structural design, air path design, and control to achieve soft and multi-mode grasping.

The main structure contains three components, including inflatable fingers, an inflatable palm, and an adapter. It has two kinds of air paths, one is applied to drive the inflatable fingers, and the other is applied to drive the inflatable palm to extend the grasping range. The control of the two air paths relies on solenoid valves and relays.

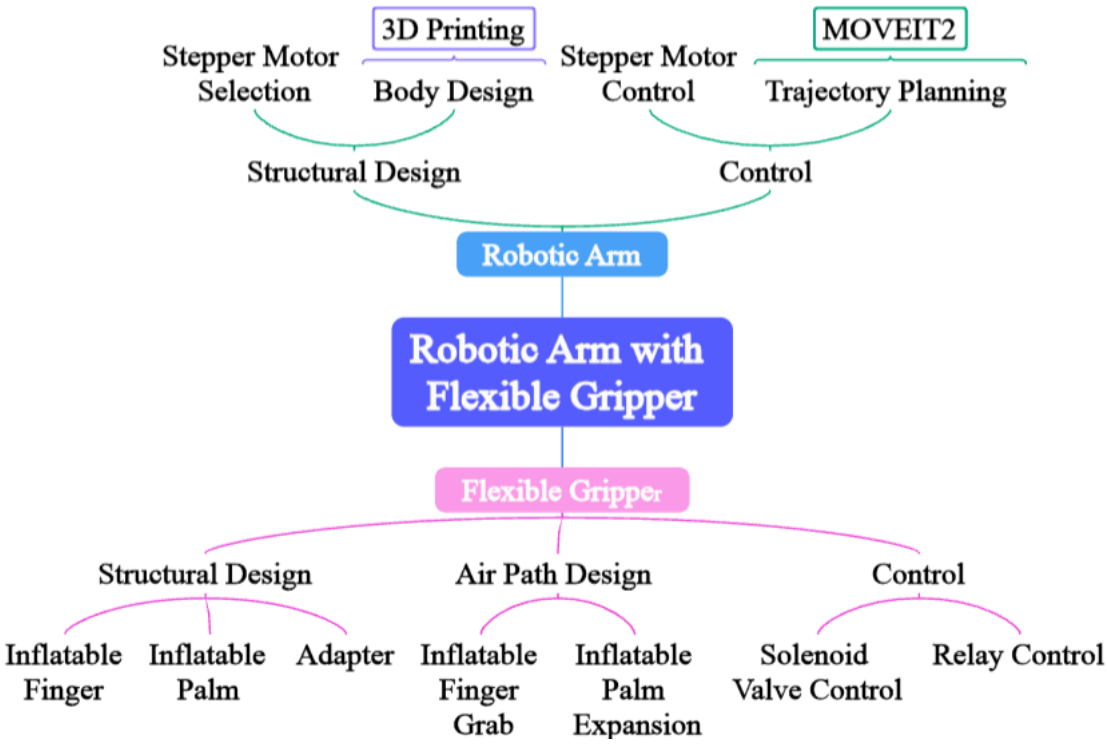

Figure 1. Design framework for the robotic arm with flexible gripper.

2.1. Robotic arm motor design

The design of the robotic arm is based on the open-source project SmallRobotArm [14]. To maximize load capacity, the structure of this robotic arm has been 3D printed, which minimizes the reliance on metal materials and reduces overall weight. Additionally, the compact design of the robotic arm helps decrease its size, allowing it to operate effectively in various environments with limited space, such as laboratories, educational settings, and light industrial applications. Despite its small size, the robotic arm has six degrees of freedom, providing it with a high level of flexibility. The components are typically designed modularly, especially the joints and end-effectors, enabling easy replacement of different end-effectors (e.g., robotic claws, suction cups, etc.) for varied tasks. Furthermore, individual components can be replaced or upgraded independently without the need to replace the entire structure.

As shown in Figure 2, the original design of the arm uses two NEMA 57 stepper motors, one NEMA 42 stepper motor, two NEMA 28 stepper motors, and one NEMA 20 stepper motor for the six joints from joint 1 to joint 6, respectively. The gripper is connected to the end of the robot arm. Since the gripper in this project is usually vertically downward, Joints 4, 5, and 6 near the end of the arm would be used as passive joints.

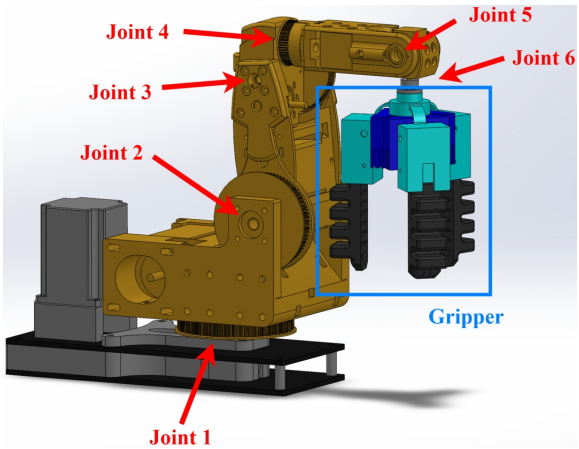

Figure 2. Modelling of six-degree-of-freedom robotic arm with the proposed flexible gripper.

The remaining 3 joints were used as active joints to control the position of the gripper. Based on the above configuration, the torque requirements of the motors for joints 2 and 3 need to be determined by calculation. Taking joint 2 as an example, the force arm reaches its maximum in the flat lifting state, and the torque requirement of the motor is also the maximum at this time.

As shown in Figure 3, the target load capacity of the designed arm is $m_L = 1$ kg, and the force arm $r_L = 227.5$ mm in the lifting position. The weight of the arm assembly on top of joint 2 is $m_A = 3$ kg, and the force arm $r_A = 91.4$ mm, with gravitational acceleration $g = 9.81$ m/s^2.

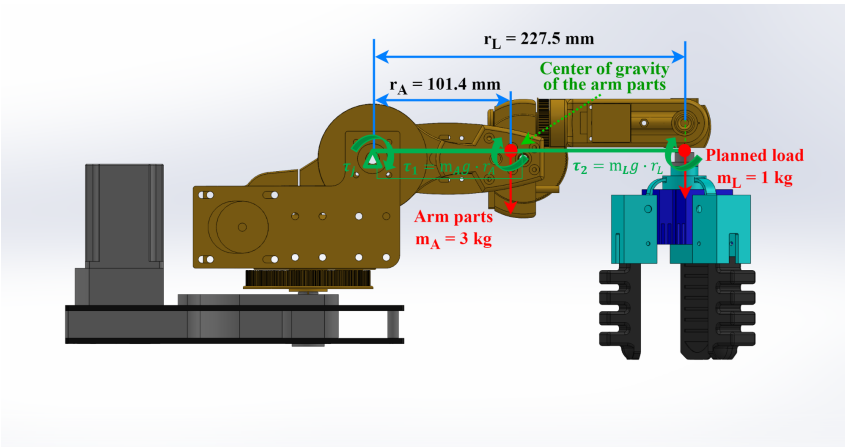

Figure 3. Key parameters of the design.

The robotic arm was designed and 3D printed by our research team. "$\tau_1 = m_A g \cdot r_A$" in Figure 3 shows the gravitational torque of the robotic arm, "$\tau_2 = m_L g \cdot r_L$" shows the rated load torque of the robotic arm, and "$\tau_j = m_A g \cdot r_A + m_L g \cdot r_L$" means that the torque of the selected motor should be torque balanced with the sum of the gravitational torque and rated load torque of the robotic arm. This is the selection and calibration criteria of the motor used in the design of the robotic arm. The motor can make the robotic arm work properly after the selection. Based on these key values, the static torque τ_j that needs to be supplied to the joints during the lifting position can be briefly calculated. The specific calculation is listed as follows:

$$\tau_j = m_L g \cdot r_L + m_a g \cdot r_A = 4.922N \cdot m \tag{1}$$

The synchronizing wheel of the motor drives the follower wheel through the timing belt to achieve rotation of the joint 2. Neglecting losses due to friction and other factors, the following calculations are carried out without considering transmission efficiency. The gear ratio of the driving wheel to the follower wheel is 24:160, from which it is possible to calculate the continuous torque τ_c that the motor needs to provide in order to keep the robotic arm raised flat.

$$\tau_c = \frac{24}{160} \cdot \tau_j = 0.7383N \cdot m \tag{2}$$

As a rule of thumb in practice, in order to lift the arm from the static position, it is necessary for the motor to provide a starting torque of approximately 2 times the static torque τ_c.

$$\tau_s = 2\tau_c = 1.4766N \cdot m \tag{3}$$

Since it is difficult for a stepper motor to provide peak torque, the maximum torque requirement of the motor, τ_s can be treated as the rated torque requirement of the motor. Therefore, Joint 2 needs to use a motor with a rated torque of at least about 1.5 N·m. According to the corresponding torque requirements for each joint, the rest of the motor will be chosen in a similar way accordingly.

2.2. Robotic arm control

In order to realize robotic arm control, this study applied MoveIt2 function in ROS2 system to control the movement. MoveIt2 consists of a functional package containing a series of mobile operations such as collision detection, manipulation control, motion planning, 3D sensing, kinematics, etc. It provides an easy-to-use platform for the development of robotic applications, evaluation of robotic designs, and architectural integration of robotics. In addition, MoveIt2 provides a range of sophisticated plug-ins that enable rapid configuration of robotic arm control and facilitate further development [15]. To visualize the movement of the robotic arm, RViz is utilized as a 3D visualization platform in the ROS2 system, which can both realize the graphical display of external information and release control information to the monitoring object. To simulate and track the movement path, the 3D model of the robotic arm is exported to the URDF file by SOLIDWORKS, then input to the Rviz environment to synchronize the real model with the simulation. Figure 4 shows the motion planning of the robotic arm model using the Moveit2 function package.

Objects need to be localized for better motion planning in RViz, The coordinates of any point Q on a rigid body in both coordinate systems can be expressed in terms of vector and direction cosines. The relationship between the two sets of coordinates is as follows:

$$x = x' \cos(x, x') + y \cos(x, y') + z' \cos(x, z') \tag{4}$$

$$y = x' \cos(y, x') + y \cos(y, y') + z' \cos(y, z') \tag{5}$$

$$z = x' \cos(z, x') + y \cos(z, y') + z' \cos(z, z') \tag{6}$$

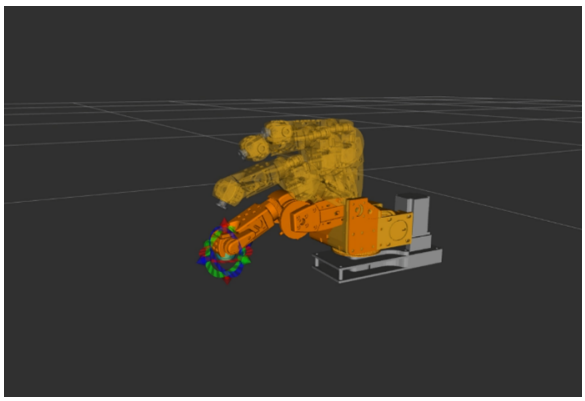

Figure 4. Kinematic simulation of the robot arm via Moveit2 in ROS.

The direction cosine matrix is used to describe the direction relationship between two coordinate systems. Equations (4), (5) and (6) describe the transformation from one coordinate system to another. x', y', z' are the coordinates of point Q in the original coordinate system, and x, y, z are the coordinates of point Q in the new coordinate system. When planning a path, MoveIt 2 needs the position and direction of the end-effector. By using a direction cosine matrix, the position and orientation of the end-effector in the local coordinate system can be converted to the position and direction in a global reference frame, such as the world coordinate system. Using the orientation cosine matrix, the exact position and orientation of the robotic arm's components in global space can be accurately calculated. When the flexible robotic arm performs a task, the robotic arm model is simultaneously co-simulated in the Rviz platform.

2.3. Flexible gripper design

2.3.1. Working principle and proposed two-step expansion algorithm

The primary structure of the flexible gripper consists of three inflatable fingers, an inflatable palm, and an adapter, as illustrated in Figure 5. The inflatable palm and inflatable fingers are controlled by separate air paths.The flexible gripper's first expansion function is realized by the inflatable palm, and the flexible gripper's second expansion function is realized by the inflatable fingers. The adapter is a connecting component that connects the inflatable palm and the inflatable fingers.

When the flexible gripper grasps the target object, it will judge the maximum radius of the target object respectively to ensure that the air pressure control fingers are adjusted to the correct grasping range. There are four cases when a flexible gripper grasps an object:

(a) Case 1: Grasp an object without using the expansion.
(b) Case 2: Grasp an object using only the first expansion.
(c) Case 3: Grasp an object using both the first expansion and second expansion.
(d) Case 4: Grasp an object using only the second expansion (Support an object internally).

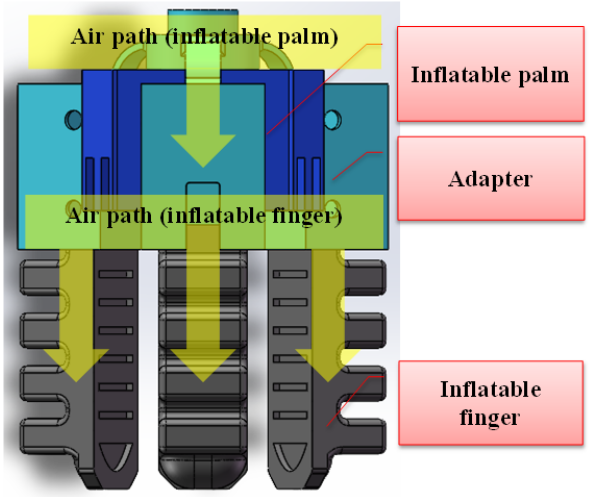

Figure 5. Key structure of the flexible gripper: Inflatable palm, adapter and inflatable fingers.

The inflatable palm's inflation realizes the first expansion and the inflatable fingers' inflation realizes the second expansion. The expansion of the flexible gripper is not activated in Case 1. In Case 2, the first expansion of the flexible gripper is activated, and the second expansion is not activated. In Case 3, both the first and second expansion of the flexible gripper are activated. As the size of the target objects increases, Cases 1-3 will be applied accordingly. The internal support function of the flexible gripper is activated in Case 4 through merely second expansion. Table 1 shows the proposed two-step expansion control logic.

Table 1. Proposed two-step expansion control logic.

Case number	Palm expansion(first expansion function)	Fingers expansion(second expansion function)
Case 1	N	N
Case 2	Y	N
Case 3	Y	Y
Case 4	N	Y

The inflatable palm's expansion is simulated and monitored to ensure accuracy across different pressure settings. The correlation between the palm's inflation and the finger's extension is tested both in simulation and physical experiments. As illustrated in Figure 6, When the flexible gripper receives a grasp signal, it derives the approximate size of the target object through the visual recognition of the camera, and executes the appropriate grasp case method according to the size of the target object. There are four types of grasp cases, each grasp case corresponds to a different target object size. The purple path indicates the usage of the flexible gripper for the inflatable palm and inflatable fingers in Case 3. Finally, the functions of the flexible gripper to hold the target object are all realized by the inflation or deflation of the inflatable fingers.

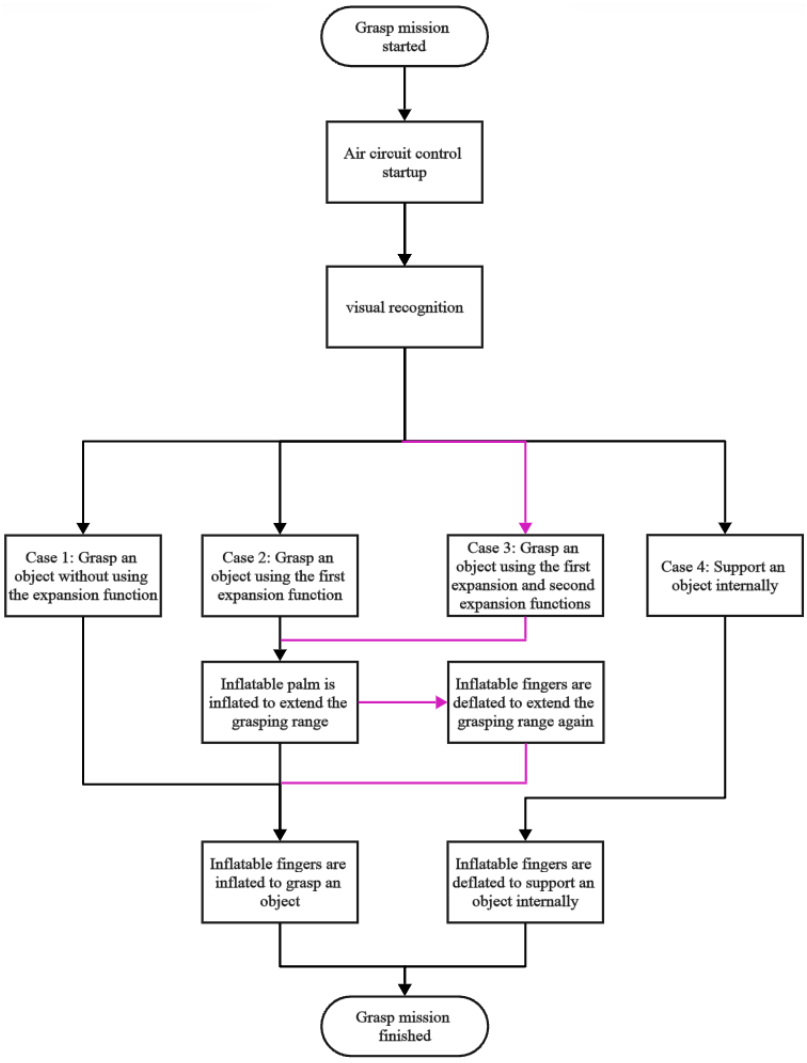

Figure 6. Flowchart of the flexible gripper control strategy.

Figure 7 shows the operating principle of controlling the position of the inflatable fingers by pneumatically actuating the inflatable palm. The key positional points of the flexible gripper are marked. A is the top centre connection point of the adapter, B is the fingertip of the inflatable finger, C is the horizontal centre point of the three fingertips, B' is the bottom midpoint of the inflatable palm side, and C' is the centre point of the inflatable palm bottom. Triangle ABC and triangle $AB'C'$ are a pair of similar triangles ($\triangle ABC \sim \triangle AB'C'$), similarity ratio is 3:1.2($\propto = 3:1.2$), so the lengths of BC and $B'C'$ have a proportional relationship. By controlling the expansion function of the inflatable palm, the length of $B'C'$ can be controlled to change, and then the length of BC can be controlled, and the first expansion range of the flexible gripper can be precisely controlled by this method. The second expansion range of the flexible gripper can be determined by controlling the pressure inside the fingers and the ductility of the material.

ΔL is the finite element simulation value. As shown in Figure 8, it is the maximum combined displacement of the inflatable palm.

$B0'C0'$ are the original radius of the flexible gripper when it is not expanded.The simulation values $B'C'$ and BC are given by:

$$B'C' = \Delta L + B0'C0' \tag{7}$$

$$BC \propto B'C' \tag{8}$$

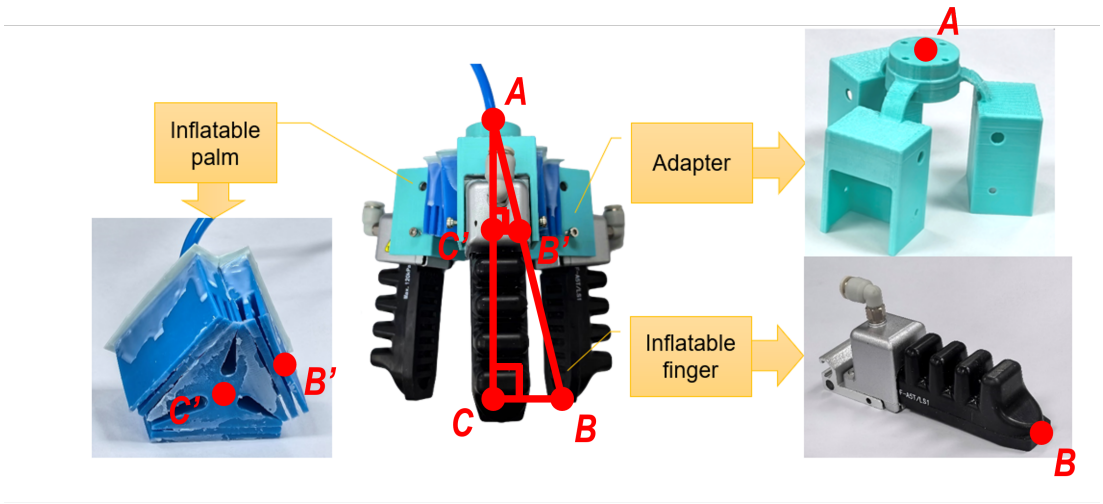

Figure 7. Geometrical modeling of grasping range.

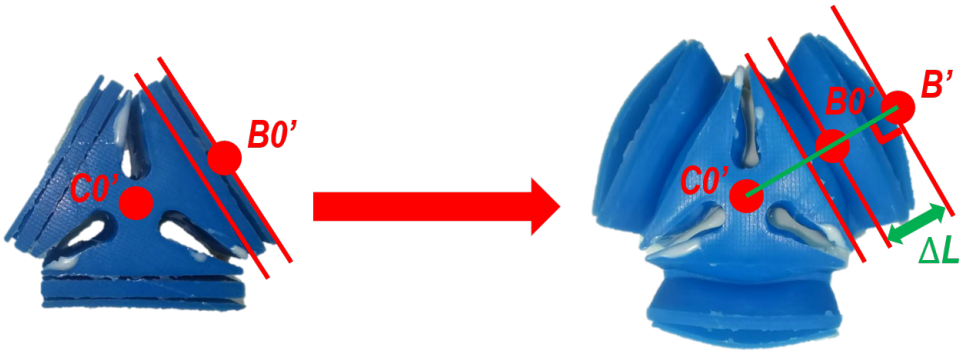

Figure 8. Overall displacement of inflatable palm.

Table 2. Simulation and experimental results of deformation and key parameters of inflatable palm with different air pressure.

Pressure value (kPa)	Maximum palm deformation (mm) $\triangle L$	$B'C'$ (mm) (Simulation)	$B'C'$ (mm) (Experiment)	BC (mm) (Simulation)	BC (mm) (Experiment)
0	0	9.75	9.75	24.37	24.55
25	7.68	17.43	17.96	43.57	44.90
30	8.47	18.22	18.90	45.55	47.25
35	9.16	18.91	19.11	47.27	47.78
40	9.75	19.50	19.78	48.75	49.45
45	10.28	20.03	20.33	50.07	50.83
50	10.50	20.25	20.77	50.62	51.93
55	11.20	20.95	21.18	52.37	52.95
60	12.61	22.36	23.56	55.90	58.90
65	13.99	23.74	24.91	59.35	62.28
70	15.34	25.09	26.34	62.72	65.85
75	15.67	27.45	28.59	68.55	71.48

Table 2 provide the maximum deformation and expansion parameters of the inflatable palm and the corresponding grasping radius of the flexible gripper under various air pressures.

2.3.2. Theoretical analysis of inflatable palm

When air pressure is increased inside a deformable, thin-walled air chamber, the imbalance in pressure between the inside and outside causes the chamber to deform. Specifically, for the inflatable palm, the chosen silicone material exhibits linear elastic deformation and is isotropic. According to Hooke's law, there is a linear relationship between stress and strain:

$$\sigma = E \cdot \varepsilon \tag{9}$$

where σ is the stress, E is the elastic modulus of the material, and ε is the strain. Thus, the air room deformation is calculated as follows:

$$\varepsilon = \frac{\sigma}{E} \tag{10}$$

In a homogeneous thin-walled air chamber, the internal pressure p induces stresses on its surface. These stresses can be classified based on their direction of action into circumferential stress along the surface and axial stress perpendicular to the surface.

$$\sigma_\theta = \frac{p \cdot r}{t} \tag{11}$$

$$\sigma_x = \frac{p \cdot r}{2t} \tag{12}$$

Where σ_θ is the annular stress, σ_x is the axial stress, p is the pressure inside the air room, r is the mean radius of the air room, and t is the wall thickness. Thus, the strain equation in different directions can be further expressed as:

$$\varepsilon_\theta = \frac{p \cdot r}{E \cdot t} \tag{13}$$

$$\varepsilon_x = \frac{p \cdot r}{2E \cdot t} \tag{14}$$

Where ε_θ is the annular strain, ε_x is the axial strain.

According to the equations, the annular strain occurring in the thin-walled air chamber is significantly larger than the axial strain under the same boundary conditions. The elastic modulus, denoted as E, also plays a crucial role in influencing the amount of strain due to the varying magnitudes of the different variables involved. The design of the inflatable palm allows its outer surface to expand during inflation, resulting in an inclined surface that helps turn the fingers outward. To achieve this design goal, it is essential to analyze and adjust the expansion rate for each part of the inflatable palm. Altering the structure and material distribution of the palm can accomplish this. By doing so, the inflatable palm can be directed to turn in a specific direction when air pressure is applied.

To enhance the horizontal expansion of the outer structure, as illustrated in Figure 9, it is essential to permit maximum annular strain in the horizontal direction. Concurrently, the air chamber at the top is

divided into continuous gully segments. When air pressure is applied, the annular strain generated on the horizontal surfaces at both ends causes the air walls on either side to tilt. This annular strain includes a horizontal component, which influences the horizontal deformation of the inflatable palm.

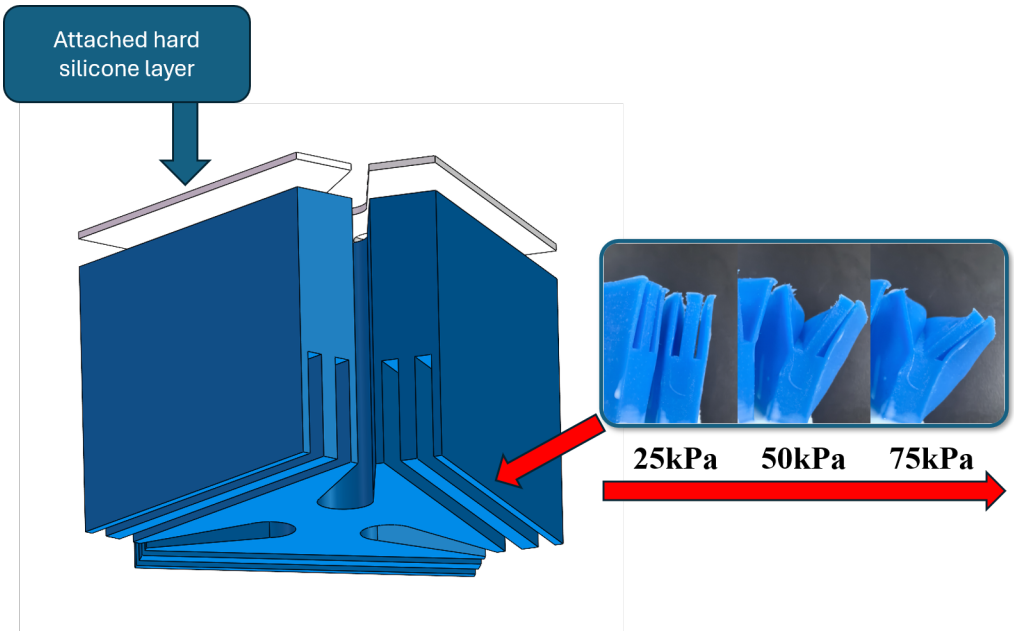

Figure 9. Structure design of inflatable palm with its expansion under different air pressure.

Furthermore, a hard silicone material, Smooth-960, is attached to the bottom of the inflatable palm. This material has a high elastic modulus, which significantly restricts the deformation of the bottom of the inflatable palm when air pressure is applied. By increasing the elastic modulus E, the annular deformation is minimized. By adjusting the expansion rates of the top and bottom sections, significant differences in their deformation under the same air pressure can be achieved. This discrepancy allows the outer surface of the inflatable palm to maintain a controlled inclination, and the resulting deformation applies pressure to the adapter, facilitating the movement of the fingers.

2.3.3. Production of flexible gripper

The primary structure of the flexible gripper consists of three inflatable fingers, an inflatable palm, and an adapter. The inflatable fingers are made from soft rubber, allowing them to bend and deform, which ensures effective object grasping. The inflatable palm inflates in a predetermined direction, thereby increasing the grasping range. In contrast to traditional fixed gripping mechanisms, this adapter has been redesigned in this study to achieve a dynamic gripping range, serving as a crucial connection between the inflatable fingers and the inflatable palm. For the fabrication of the inflatable palm, silicone materials Mold Star 30 and Smooth-Sil 960 are used. The molds are created using 3D printing, and these molds are later utilized in a molding process to produce the gripper components.

The fabrication process of the flexible inflatable palm is illustrated in Figure 10. Each component of the mold for the inflatable palm has a centrally symmetrical cross-section so that the components have the same coincident central axis. Three positioning holes in the same plane are fitted to determine the position of the parts in the plane, thus ensuring that the center axes coincide. The multiple positioning holes also ensure the mold wall with uniform thickness, maintaining the typical mechanical properties. The molding

material is poured into the designed mold, and upon solidification, a completed capped inflatable palm can be prepared, leaving the bottom of the inflatable palm unsealed. To achieve a closed cavity, the body needs to be sealed by an additional process.

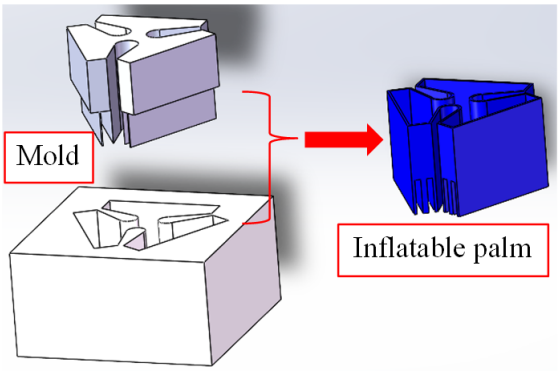

Figure 10. Mold design of the inflatable palm.

When the flexible gripper requires an extension of its grasping range, the inflatable palm begins to expand with air pressure. Such expansion force would result in the adapter's surface deformation. The grasping range will be further expanded as a result of the deformation of the adapter, which will finally increase the distance between inflatable fingers to the centre. To smooth the expansion, a curved structure of the adapter is optimized as Figure 11. The simulated value for different thicknesses of the curved structure is in Table 3, the displacement means the increased radius of the adapter expansion under the corresponding forces. *N.A.* reflects a broken connection. After analysis, it is found that the main reason for the breakage is the stress concentration phenomenon in some localized areas of the adapter. In areas where the load is not uniformly distributed, the local stress is much higher than the average stress. The stress concentration leads to a rapid increase in strain in these areas, which exceeds the yield limit of the material, leading to plastic deformation and a gradual loss of load carrying capacity. Under high loads or fatigue, cracks appear and expand in these stress concentration areas, eventually leading to the overall fracture of the adapter. Moreover, the mechanical properties of these areas are significantly weakened by the stress concentrations, and even if the overall structure does not fail completely, these weak points are prioritized for damage and become the start point of breakage. For example, with a thickness of 2 mm, this curved structure allows the adapter to generate large deformation with weak pressure, a 5 N stress will result in a 11.7 mm extension of the gripper radius range. At the same time, the curved structure prevents the adapter from damage under stress concentration.

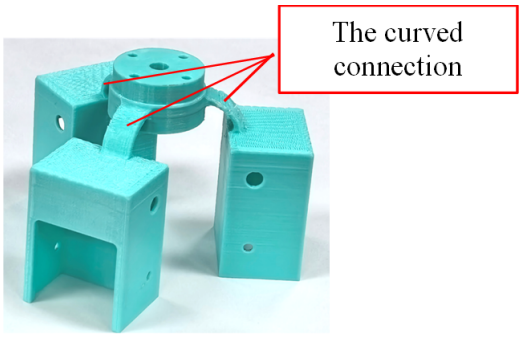

Figure 11. 3D printed adapter with curved connection.

Table 3. Thickness optimization for adapter's curved structure.

Thickness	1 mm			
Simulated Force	1 N	3 N	5 N	7 N
Expansion	28.56 mm	*N.A.*	*N.A.*	*N.A.*
Thickness	2 mm			
Simulated Force	1 N	3 N	5 N	7 N
Expansion	2.38 mm	7.10 mm	11.71 mm	16.14 mm
Thickness	3 mm			
Simulated Force	1 N	3 N	5 N	7 N
Expansion	1.04 mm	3.12 mm	5.19 mm	7.24 mm

2.4. Air path control design

According to the designed gripper, the pneumatic air path design contains two parts to control the inflatable palm and inflatable fingers. The air path design for inflatable fingers includes the same type of components as depicted in Figure 12(a), while the difference is a negative pressure condition is needed, which requires a second path as Figure 12(b). As shown in Figure 12(a), the red labelled air path illustrates the positive pressure for griping manipulation, the blue labelled air path in Figure 12(b) is activated to allow inflatable fingers in a reverse bending state with negative pressure, which may realize internal support function for objects like containers and boxes.

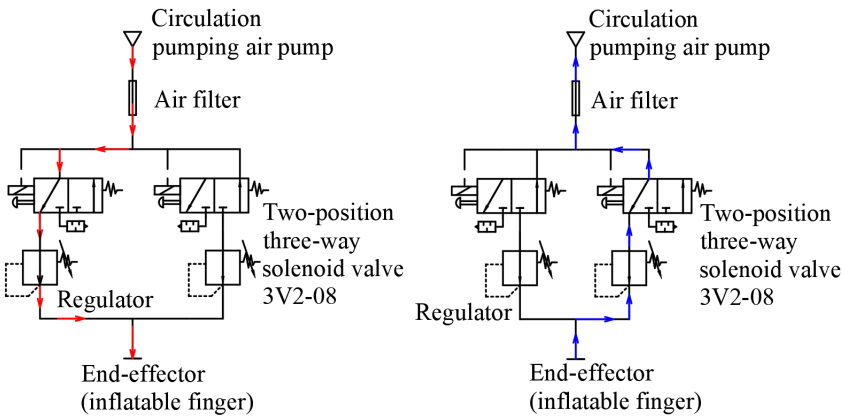

Figure 12. Air path design of inflatable fingers. **(a)** Positive pressure environment air path design and gas flow direction. Gas is routed by the red line from the pump through the gas filter, solenoid valve, regulator and finally to the end-effector (inflatable finger). **(b)** Negative pressure environment air path design and gas flow direction. The gas is pumped from the blue line by a gas pump.

The inflatable finger is designed to control the airflow necessary for grasping or providing internal support to objects. To ensure safety and precise air pressure regulation, this system includes the following components: air pump, air filter, solenoid valve, regulator, and flexible gripper. When the solenoid valve is activated, the air chamber shifts, opening a pathway for positive air pressure. The regulator then adjusts the pressure to the desired working state. As a result of this pressure difference, air flows into the inflatable finger, causing it to bend as the internal pressure increases. This bending action enables the finger to grasp the target object. Once the regulator sets the air pressure to the working level, the air continues to fill the

inflatable finger, leading to further downward bending due to the internal pressure. When the air pump is turned off, the pressure equalizes back to atmospheric levels. Air then escapes through the muffler plug on the solenoid valve. Consequently, the object is released by gravity, and the finger returns to its original shape as the bending deformation ceases.

Simultaneously, the air path control design of the inflatable palm uses the component connection method of "air pump - air filter - solenoid valve - regulator - inflatable palm". When the air source is activated, the air enters the air path, and the air filter cleans the air. When the solenoid valve is energized, the left air chamber replaces the right air chamber into the air path, and then the left air path is opened. When the size of the object being grasped by the flexible gripper exceeds the maximum grasping range of the inflatable fingers, the ability of the inflatable palm and adapter to expand in a specific direction can enhance the grasping range of the flexible gripper. Figure 13 illustrates a diagram of the air path of the inflatable palm expanding in the intended direction in a positive pressure environment.

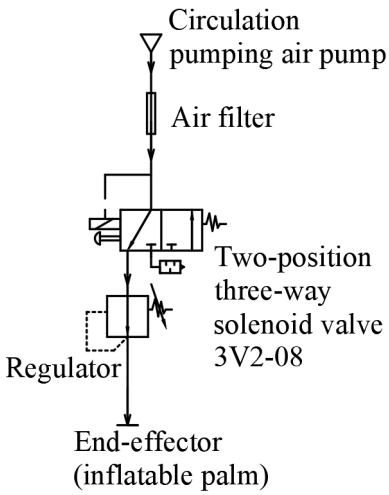

Figure 13. Air path design of inflatable palm.

3. Simulation and experimental results

3.1. Inflatable palm and finger

The simulation experiment of the flexible gripper includes both the palm and fingers expansion range under varied pressure environments. The purpose of this simulation is to test the feasibility of the corresponding designs. To optimize the design of the inflatable palm and fingers, finite element analysis (FEA) was performed to test the required kinematics and deformation. This design is inspired from a previous finger design [16]. However, in this study, the geometry and internal structure of the finger are modified to meet our robot's manipulation requirement.

The air enters the chamber when the solenoid valve is activated with the air source, resulting in the inflatable palm expanding in a predetermined direction. The simulation results in Figure 14 show a specific displacement gradient across the structure of the inflatable palm under 50 kPa positive pressure. The legends in the images represent displacement values (notated as URES, in mm), indicating how much each part of the structure has deformed from its original position. Different colours on the scale correlate to different magnitudes of displacement. At the top of the dome, where displacement values

reach up to approximately 10.6 mm, the material exhibits considerable deformation due to the internal pressure pushing outward. Conversely, the base of the palm shows minimal displacement, maintaining stability and anchoring the structure. Simulation data shows that the outer surface of the inflatable palm can be effectively deformed towards the target direction under positive pressure, thus driving the flip of the fingers. Meanwhile, the displacement of each lateral side of the inflatable palm was increased from the edge to the middle position. This reaches the displacement limit of the inflatable palm.

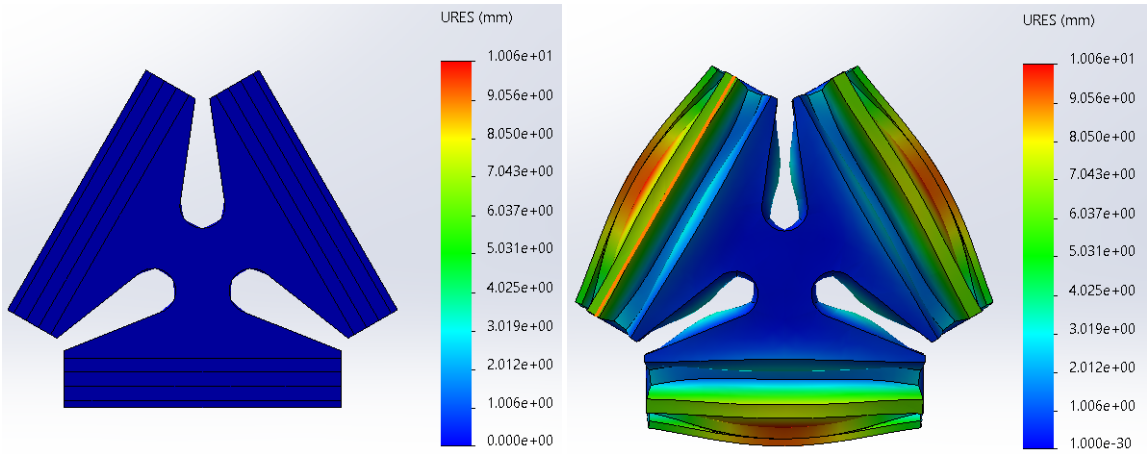

Figure 14. Simulation results of inflatable palm. **(a)** The initial state when the inflatable palm does not start to inflate, **(b)** The maximum displacement of the inflated palm was 10.6 mm at 50 kPa.

As demonstrated in Table 4, Mold Star 30 allows a maximum palm deformation of 10.5 mm at a standard pressure of 50 kPa. This deformation is significant compared to Nylon, which only deforms by 0.57 mm under the same conditions, illustrating that materials with high stiffness (like Nylon) provide insufficient flexibility, resulting in minimal deformation. This rigidity hinders the gripper's ability to adapt its shape to grasp various objects effectively. *N.A.* indicates that the hydrogel cannot stand the air pressure of 50 kPa, resulting in breakage. Compared with hydrogel, Mold Star 30 has soft characteristics while its toughness can also support it to complete the elastic deformation.

Table 4. Maximum deformation of inflatable palms under different materials at 50 kPa.

Material name	Maximum palm deformation (mm)
Mold star 30	10.5
Nylon	0.57
Hydrogel	*N.A.*

Figure 15(a) shows the simulation result of a deformed inflatable finger under 75 kPa positive pressure. The tip of the inflatable finger showed the largest displacement, approximately 14.88 mm, which indicates that this component stretched considerably when it was pressurized. The gradient of displacement decreases towards the base, which remains more stable and experiences far less stretching. This pattern of deformation underlines the differential response of the finger's segments to internal pressure, indicating that the inflatable finger can satisfy a reliable connection of its base to an adapter and still have a sizable amount of deformation at its tip.

In contrast, the deformation of the inflatable finger in the negative pressure environment is illustrated in Figure 15(b). The 0.5-atmosphere negative pressure operation leads to the highest displacement observed in the tip of the pneumatic finger, reaching up to 26.31 mm. This significant inward displacement indicates a strong compression force, causing the tip to collapse inward.

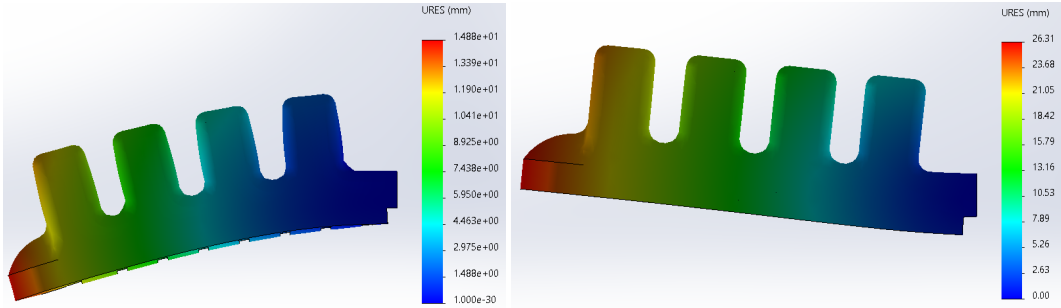

Figure 15. Simulation results of the inflatable finger. **(a)** The maximum displacement was 14.88 mm at a positive pressure of 75 kPa. **(b)** The maximum displacement was 26.31 mm at a negative pressure of 0.1 atmosphere.

Figure 16 shows the finite element simulation analysis of the adapter made from 3D-printed raw material in ABS. The purpose of this simulation is to check the strength of the adapter. The maximum displacement of the adapter reaches 11.71 mm at a thickness of 2 mm for the curved structure of the adapter, which does not break due to stress concentration and meets the working requirements of the flexible gripper to grasp the object.

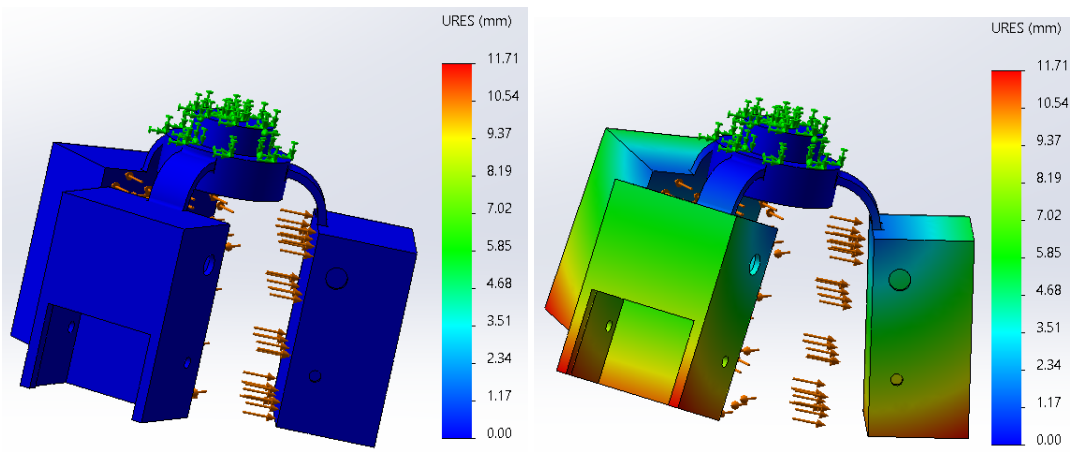

Figure 16. Finite element simulation and analysis experiment of adapter. **(a)** The initial state when the adapter is not forced, **(b)** The maximum displacement was 11.71 mm under a force of 5 N.

3.2. Preliminary test of flexible gripper

Figure 17, showcasing the palm inflated and expanded multiple times in a controlled setting, reflects minimal variability in the measurements. This consistent repeatability is crucial, as it substantiates the reliability of the inflatable palm for practical applications, ensuring that the device performs predictably under different conditions.

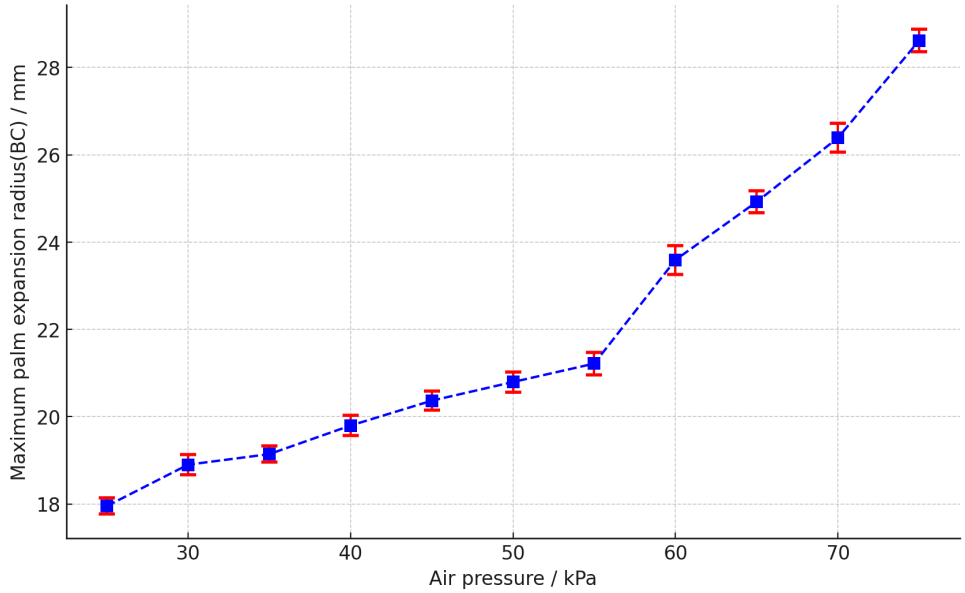

Figure 17. Error bar of the grasping radius at different air pressures caused by inflatable palm expansion.

Figure 18 depicts the comparison between the simulation and experimental results of the inflatable finger under varying air pressures. Points 1-5 are located at the same horizontal distance, while point 6 is positioned at the tip of the inflatable finger, exhibiting different vertical and horizontal distances compared to the other points. As a result, the variation in the X and Y positions of point 6 is smaller than that of the other points. L represents the length of the inflatable finger. This figure shows the consistency and effectiveness of fingers' variation.

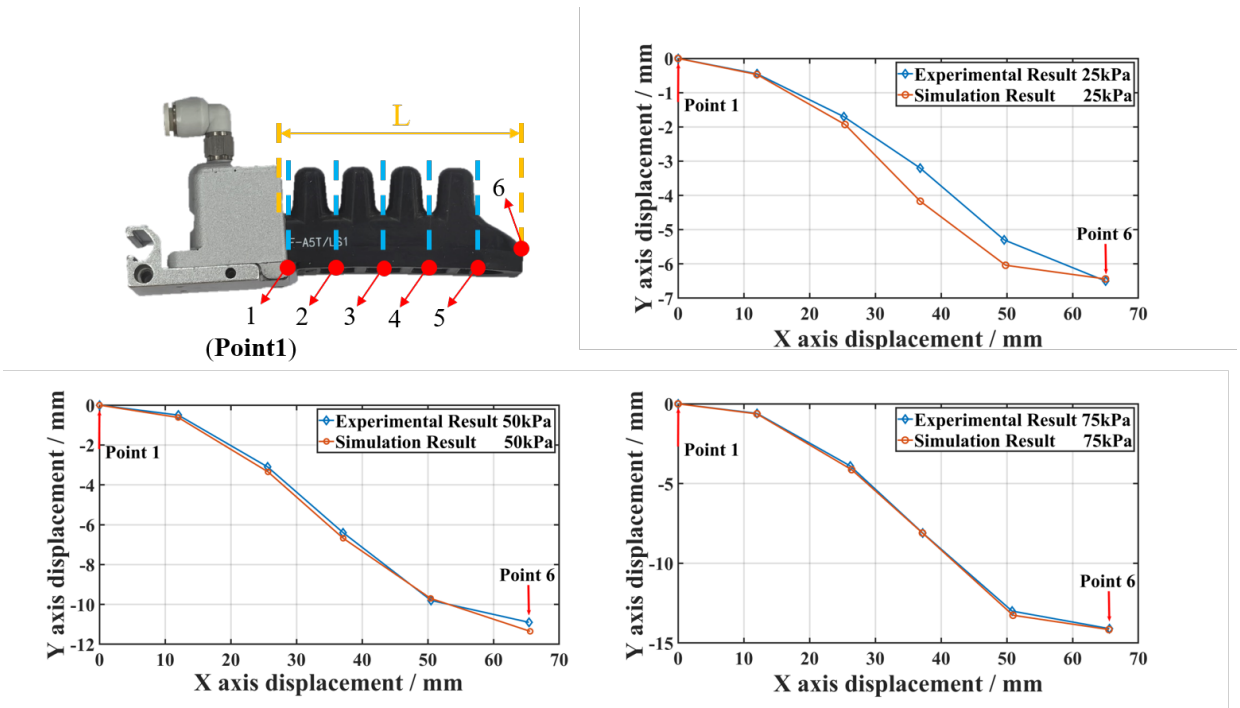

Figure 18. Simulation and experimental results of inflatable finger under different pressure.

The differences at lower pressures primarily result from simulation limitations and visual exaggeration

in the graph. Simulations use simplified material models and geometries to reduce computational complexity, which may not fully capture real-world variations caused by material imperfections, manufacturing inconsistencies, or environmental factors. Additionally, the scaling of the y-axis in Figure 18 visually amplifies discrepancies, but the actual maximum deviation is only about 1mm (approximately 8% of total deformation), which is minimal and does not significantly impact performance. It is also worth noting that the gripper rarely operates at such low pressures (around 25 kPa) in practical applications, where higher pressures align better with simulation results. Therefore, these minor discrepancies are within an acceptable range and do not affect the gripper's functionality under normal working conditions.

In summary, while finite element simulations serve as a valuable tool for predicting the behavior of the gripper, discrepancies between simulation and experimental results can arise due to factors such as material property variations, simplified geometrical assumptions, boundary condition differences, and experimental measurement uncertainties. The overall trends and behaviors observed in the experiments align well with the simulated predictions.

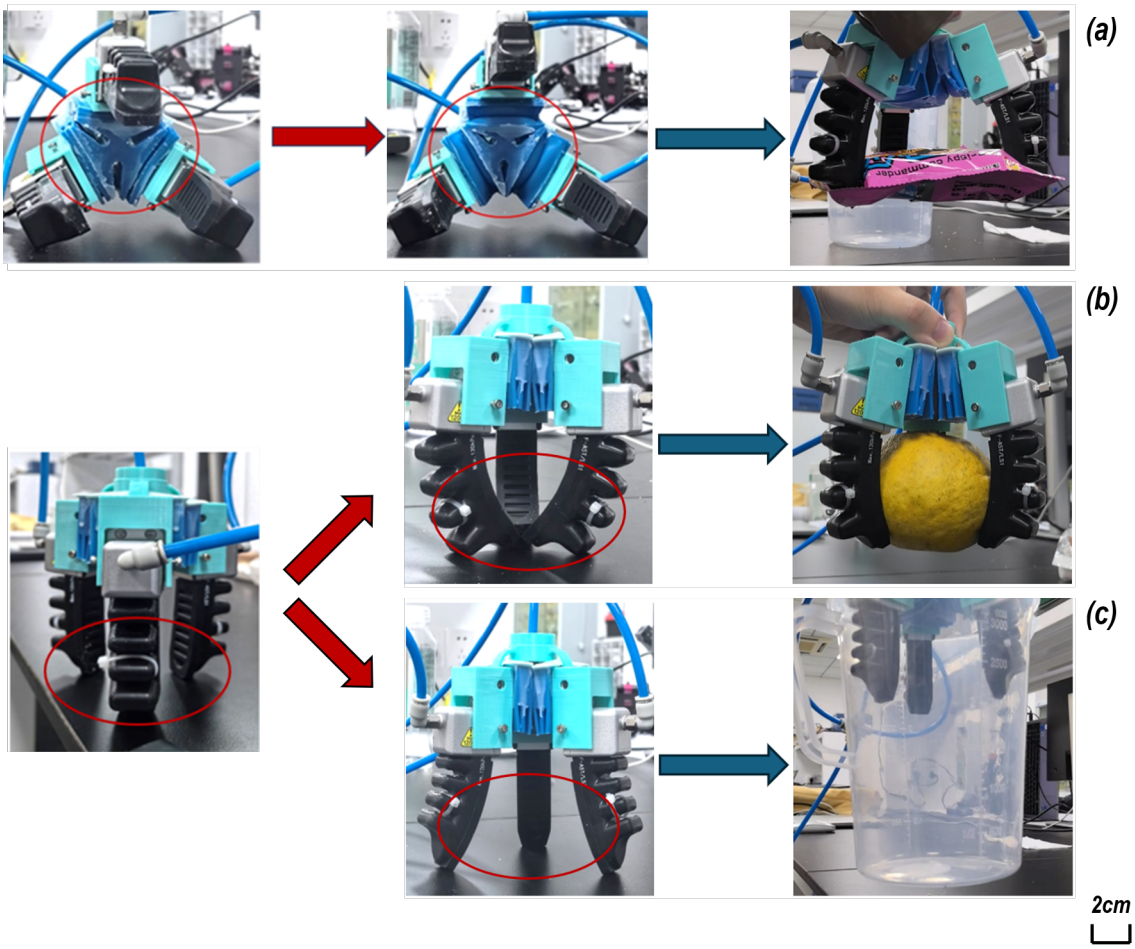

Figure 19. Preliminary tests for flexible gripper. **(a)** Case 3, **(b)** Case 1, **(c)** Case 4.

Figure 19 shows the flexible gripper grasping different objects under positive or negative pressure. The Raspberry Pi GPIO is responsible for the automatic control of the electrical signal in the air path by regulating the solenoid valve, which controls the relay in turn and sends out the electrical signal to open and close the valve. Specifically, when the air pump activates, as shown in Figure 19(a), the pressure in the inflatable palm increases, which expands the adapter in a predetermined direction to increase the reaching

gripping range, resulting in a dynamic gripping radius from 4cm to 7cm. The maximum displacement position of the inflatable palm occurs in the middle of the lateral position, which provides the same results in the simulation stage. To test the capability of fingers, one 500 grams grapefruit with 11 cm diameter and one 9 cm-radius pot were tested, as shown in Figure 19(b)and (c), respectively, the former tests the gripping capability, while the latter shows the function of internal support under negative pressure. The maximum displacement of the inflated finger in both positive and negative pressure environments occurred at the fingertip. All the testing results are aligned with theoretical analysis, which proved the effectiveness of the designed flexible gripper.

Table 5 categorizes the objects grasped by Three-dimensional data, shape, mass, hardness and the required grasping radius. For instance, the table lists objects ranging from a flattened instant noodle bag to a granular spherical glutinous rice ball, covering a variety of shapes such as spherical, cup-shaped, and flattened. The masses of these objects vary from as light as 50 grams to as heavy as 800 grams. They also have different 3D data and Shore hardness. The grasping radius needed for these objects also spans from 45 mm to 65 mm, demonstrating the gripper's ability to adjust its grip based on the size and shape of the object.

Table 5. Experimental grasping results for different sizes and hardnesses of objects.

Grasping result	Target object name	Three-dimensional data(cm)	Shape type	Mass(g)	Shore hardness	Grasping radius range(mm)
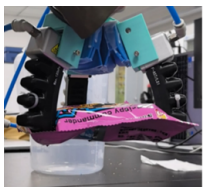	Instant noodle bag	12*12*5	Flattened	110	Shore A 30	65
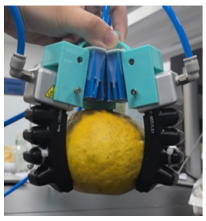	Grapefruit	5.5 cm-radius	Spherical	500	Shore A 20	55
	Bucket	9 cm-radius	Cup-shaped	50	Shore D 40	55
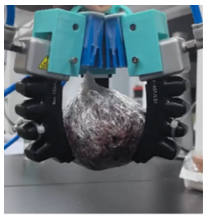	Sticky rice ball	4 cm-radius	Granular spherical	800	Shore A 10	45

4. Conclusion

This paper presents the development of a flexible gripper featuring a novel, adjustable dynamic grasping range. Unlike conventional approaches that require manual adjustment, the proposed design incorporates a pneumatic inflatable palm to precisely control and expand the grasping range, thereby enhancing the gripper's overall grasping capability. Additionally, a two-step expansion algorithm has been proposed to control the grasping range more precisely. While the current design faces certain limitations, such as the relatively short lifespan of 3D-printed materials and the non-uniform thickness of the silicone-based palm, experimental results have demonstrated the effectiveness and feasibility of the proposed gripper design.

Acknowledgment

This research has been supported in part by Xi'an Jiaotong-Liverpool University (XJTLU) Teaching development fund under Grant (TDF20/21-R22-144, TDF22/23-R25-198), and in part by XJTLU Research Development Fund under Grant (RDF-22-01-081, REF-21-02-001).

Author's contribution

Please make specific attributions of author contribution and responsibility in this part and follow CRediT to define the roles of co-authors. The following statements should be used "Conceptualization, X.X. and Y.Y.; methodology, X.X.; software, X.X.; validation, X.X., Y.Y. and Z.Z.; formal analysis, X.X.; investigation, X.X.; resources, X.X.; data curation, X.X.; writing—original draft preparation, X.X.; writing—review and editing, X.X.; visualization, X.X.; supervision, X.X.; project administration, X.X.; funding acquisition, Y.Y. All authors have read and agreed to the published version of the manuscript.".

References

[1] Wang J, Lu Y, Song C, Xu B, Bu Q, *et al.* Design of Flexible Gripper with Inflatable Palm for Dynamic Grasping Range. In *2024 29th International Conference on Automation and Computing (ICAC)*. 2024 pp. 1–7.

[2] Lu Y, Liu Y, Bu Q, Lim EG, Devaraj R, *et al.* An Autonomous Vehicle Platform for Parcel Delivery. In *2023 28th International Conference on Automation and Computing (ICAC)*. 2023 pp. 1–7. 10.1109/ICAC57885.2023.10275203.

[3] Liu Y, Lu Y, Peng C, Bu Q, Liang YC, *et al.* Autonomous Vehicle Based on ROS2 for Indoor Package Delivery. In *2023 28th International Conference on Automation and Computing (ICAC)*. 2023 pp. 1–7. 10.1109/ICAC57885.2023.10275227.

[4] Li K, Xu Y, Zhao Z, Li A, Meng MQH. Closed-Loop Magnetic Manipulation for Robotic Transesophageal Echocardiography. *IEEE Transactions on Robotics* 2023 39(5):3946–3959. 10.1109/TRO.2023.3281477.

[5] Kurundkar S, Kshirsagar K, Kulkarni V, Lambat H, Lambe M. 3D Printed Robotic Arm using Hand Gestures. In *2023 7th International Conference on I-SMAC (IoT in Social, Mobile, Analytics and Cloud) (I-SMAC)*. 2023 pp. 1087–1094. 10.1109/I-SMAC58438.2023.10290643.

[6] Koban N, Çavli N, Doğan H, Benli E. 7 DOF Robotic Arm Inverse Kinematic Analysis with Cuckoo

and Whale Algorithms. In *2023 Innovations in Intelligent Systems and Applications Conference (ASYU)*. 2023 pp. 1–5. 10.1109/ASYU58738.2023.10296820.

[7] Al Mhdawi AK, Wright N, Humaidi AJ, Azar AT. Adaptive PI-Fuzzy Like Control of a Stack Pneumatic Actuators Testbed for Multi-Configuration Small Scale Soft Robotics. In *2023 International Conference on Manipulation, Automation and Robotics at Small Scales (MARSS)*. 2023 pp. 1–8. 10.1109/MARSS58567.2023.10294122.

[8] Yiyang H. Design and fabrication, simulation test and application investigation of a new pneumatic soft actuator. Master's thesis, Hunan University, 2019.

[9] Gonzalez J, Poza J, Robles J, Ponce H, Brieva J, *et al.* Design of a Soft Gripper Hand for a Quadruped Robot. *2023 IEEE 15th International Symposium on Autonomous Decentralized System (ISADS), Autonomous Decentralized System (ISADS), 2023 IEEE 15th International Symposium on* 2023 pp. 1 – 6.

[10] Gulnergiz ET, Dilibal S, Gormus B, Danquah JO, Emon OF. Additively Manufactured Soft Pneumatic Gripper Integrated Remotely Operated Underwater Vehicle (ROV) for Grasping Archeological Remains. In *2023 5th International Congress on Human-Computer Interaction, Optimization and Robotic Applications (HORA)*. 2023 pp. 01–05. 10.1109/HORA58378.2023.10156774.

[11] Heeringa W, Santina CD, Smit G. FinFix: A Soft Gripper With Contact-Reactive Reflex for High-Speed Pick and Place of Fragile Objects. In *2023 IEEE International Conference on Soft Robotics (RoboSoft)*. 2023 pp. 1–7. 10.1109/RoboSoft55895.2023.10122107.

[12] Shize Y, Zhouyi W, Zhendong D, Bingcheng W, Yu G, *et al.* Design of a bionic flexible robotic arm for aerospace requirements. *Mechanical Manufacturing and Automation* 2020 (1):134–137.

[13] Yoder Z, et al. A soft, fast and versatile electrohydraulic gripper with capacitive object size detection. *Advanced Functional Materials* 2023 33(3):2209080. 10.1002/adfm.202209080.

[14] nd. GitHub - SkyentificGit/SmallRobotArm: This is the open source project of the 6DoF robot arm based on stepper motors.

[15] Coleman D, Sucan I, Chitta S, Correll N. Reducing the Barrier to Entry of Complex Robotic Software: a MoveIt! Case Study. 2014 .

[16] Jain S, Dontu S, Teoh JEM, Alvarado PVY. A multimodal, reconfigurable workspace soft gripper for advanced grasping tasks. *Soft Robotics* 2023 10(3):527–544.